ACS Sustainable Chemistry & Engineering

pubs.acs.org/journal/ascecg

Research Article

Electrocatalytic Reduction of Aldonic Acids to Aldoses on Gold Electrodes

Maria Wolfsgruber, Bruno V. M. Rodrigues, Marcia Gabriely da Cruz, Robert H. Bischof, Serhiy Budnyk, Björn Beele, Susanna Monti, Giovanni Barcaro, Christian Paulik,* and Adam Slabon*

Cite This: https://doi.org/10.1021/acssuschemeng.2c05576

Read Online

ACCESS | Metrics & More | Article Recommendations | Supporting Information

ABSTRACT: Spent sulfite liquor, a side-stream from the pulp and paper industry, is an abundantly available carbon source for bio-based platform chemicals. The biotechnological valorization of side streams in biorefineries is hampered by the inability of many microorganisms to metabolize and deal with aldonic acids. Based on the principles of *Green Chemistry*, the electrochemical reduction of aldonic acids into the corresponding biomass sugars appears as a prospective process for the conversion of these acids into fermentable carbohydrates. In our paper, the investigation of electrochemical reduction of gluconic and xylonic acids into glucose and xylose, respectively, is presented. The proposed mechanism on a gold-coated silver electrode was determined *via* ReaxFF molecular dynamics simulations and quantum chemistry calculations. Model solutions with an aldonic acid concentration of 2.5 wt % were used for the experiments. Compared to a two-electrode compartment cell, the amounts of glucose and xylose produced in the undivided cell were more than 4 and 5.5 times higher, respectively. The electrode surface was analyzed by scanning electron microscopy, energy-dispersive X-ray spectroscopy, and X-ray photoelectron spectroscopy. Despite the relatively low conversion rate, our results show that electrochemical reduction of aldonic acids into their corresponding aldoses in model solutions is possible, which represents an important step toward side-stream valorization.

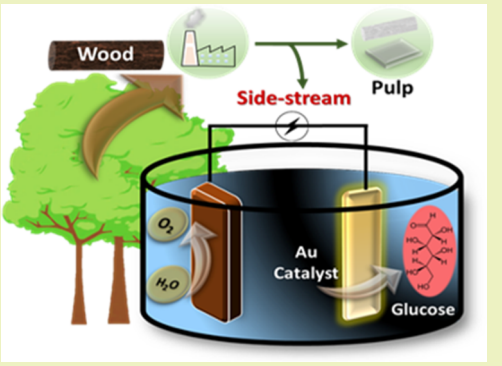

KEYWORDS: *gold, spent sulfite liquor, gluconic acid, xylonic acid, glucose, xylose*

INTRODUCTION

Economic and ecological aspects have led the industry to focus on not only process optimization but also side-stream valorization.[1] In this context, biorefineries represent one of the main opportunities to achieve global climate goals and harness side streams while presenting a way to replace petroleum-based chemicals with renewable raw materials.[2] In this respect, spent sulfite liquor (**SSL**) is an abundant side-stream in the pulp and paper industry, which is rich in various carbon sources that can serve as a feedstock for several bio-based platform chemicals. This side-stream consists mainly of different wood degradation products, for example, soluble carbohydrates in the form of sugars, lignosulfonates, and aldonic acids.[3,4] The latter are formed during the reaction of aldoses in oxidative environments. In the sulfite pulp process, oxidation occurs mainly in the process step of glycosidic cleavage of hemicellulose chains.[5,6]

In many biorefineries, the use of SSL is limited due to the inhibitory effect of some components, for example, aldonic acids.[7] The successful fermentation of SSL is hampered by the presence of aldonic acids and water-soluble lignosulfonates, which must be removed from the side-stream.[8−10] Extraction, adsorption, membrane separation, and precipitation are examples of techniques used to separate lignosulfonates. Contrariwise, similarities in the structure, size, and properties between aldonic acids and their corresponding sugars make their separation challenging and costly on an industrial scale.[11−14] Therefore, the possibility of converting these side-products into more valuable carbohydrates appears to be a more prospective approach. In the context of circular economy, it is also desirable to add value to aldonic acids in the pulp processing cycle.[1]

The reduction of aldonic acids into the corresponding sugars or alditols is a strategy to valorize these acids. In 1927, Glattfeld and Shaver reported on the conversion of gluconic acid to glucose *via* catalytic hydrogenation in the presence of glucose. Catalytic reduction with hydrogen on platinum black as a catalyst led to a conversion rate of 14−28%. However, the reactivities of other aldonic acids, such as mannonic and galactonic acids, were quite different, and the conversion to the corresponding sugars could not be achieved to the same

Received: September 16, 2022
Revised: November 22, 2022

Scheme 1. Schematic Illustration of the Electrochemical Reduction of Aldonic Acids to the Corresponding Sugars in Different Cell Geometries on Gold-Functionalized Electrodes

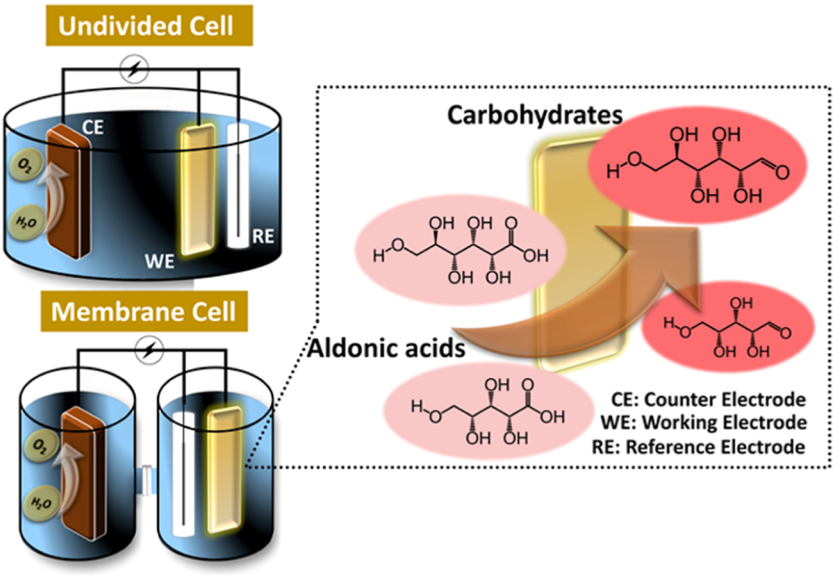

extent.[15] A method for the separation of a mixture of xylonic acid and xylose from SSL, including subsequent fractionation of these substances, has also been reported.[16] The resulting fractions, one richer in xylose and the other in xylonic acid, can be further catalytically hydrogenated to xylose and xylitol. This hydration process requires a metal hydride as a catalyst and the reaction temperature and pressure in the range of 100−130 °C and 100−130 bar, respectively.[16] However, safety concerns and environmental impacts make the combination of chromatography and hydrogenation at high pressures and temperatures not sustainable.[17,18]

The low selectivity of the direct catalytic hydrogenation of SSL would result not only in the conversion of the aldonic acid but also in the reduction of different components in the SSL. Another disadvantage is the potential poisoning of the catalysts by the sulfur components in the SSL. Consequently, selective hydrogenation to specific products is, in general, highly challenging.[1,19] A more benign approach could, however, be the application of electrocatalytic reduction using *Green Chemistry* principles.[20−23] A range of electrochemical syntheses for the valorization of carbohydrates has been investigated. Park *et al.* and Pintauro *et al.* reported on the electrochemical oxidation and reduction of glucose to gluconic acid and sorbitol.[24,25] Governo *et al.* elaborated on the electrochemical oxidation of xylose to xylonic acid in an alkaline medium.[26] Electrochemical degradation of lignin to high value-added products has been exploited since the 20th century and remains popular,[27−32] because of its high yield of aromatic compounds and carbohydrates, which can serve as feedstock for various platform chemicals.[1,4,33,34]

To date, only few studies have been dealing with electrocatalysis in biotechnological applications; therefore, the variety of products is still low. There are some studies in the field of fuel and chemical production with microbial electrocatalysis in redox biosynthesis, like the reduction of carbon dioxide to acetate as biofuel.[35] Reactions of glucose with sequential fermentation and electrocatalytic reduction to 3-hexenedioic acid have been achieved with a yield of 67% and high selectivity.[36] While being an underexplored field, these studies in biomass transformation and valorization demonstrate the high potential of electrocatalysis within the (bio)-technological field.

While previous reports have focused on the valorization strategies of various carbohydrates, the electrochemical reduction of aldonic acids to the corresponding sugars has not yet been reported. In this investigation, we disclose a straightforward and sustainable approach to the electrocatalytic reduction of aldonic acids using gold-functionalized electrodes (Scheme 1).

EXPERIMENTAL SECTION

Materials. D-Gluconic acid (50%) was purchased from Alfa Aesar. (3*R*,4*R*,5*R*)-3,4-Dihydroxy-5-(hydroxymethyl)-tetrahydrofuran-2-one was purchased from ChiroBlock GmbH. Tetrachlorauric(III) acid ($HAuCl_4$) trihydrate and the hydrochloric acid (37%) were purchased from Acros Organics, whereas both the silver wire (1.0 mm, 99.9%) and gold wire (0.5 mm, 99.95%) were purchased from abcr GmbH. The Fumapem F-10100 cation exchange membrane was purchased from Fumatech BWT GmbH. Magnesium sulfate ($MgSO_4$) was acquired from Mallinckrodt and sulfuric acid (H_2SO_4, 95%), sodium chloride, sodium hydrogen carbonate, and nitric acid (65%) from VWR. The platinum mesh and the potassium chloride (KCl) were purchased from VWR. The Toray carbon paper T-060 was purchased from Quintech. Deionized (DI) water and Milli-Q water were used in all experiments.

Solutions. Aldonic acid solutions (AAS) were prepared by dissolving the corresponding amount of aldonic acid in DI water. As an electrolyte, $MgSO_4$ was dissolved separately in DI water, and then the two solutions were combined. The mixture was then filled up to the total amount of the final solution (100 g) with DI water and adjusted to the desired pH value of 2.5 with H_2SO_4. The different solutions are listed in Table 1. In order to test whether the setup

Table 1. Summary of the AAS Prepared with Different Aldonic Acids (AA) and Concentrations of the Aldonic Acids [*w*(AA)] and Electrolyte [*w*($MgSO_4$)]

name	aldonic acid	*w*(AA)/wt %	*w*($MgSO_4$)/wt %
G1	gluconic acid	2.5	1.5
X1	xylonic acid	2.5	1.5

https://doi.org/10.1021/acssuschemeng.2c05576
ACS Sustainable Chem. Eng. XXXX, XXX, XXX−XXX

works for other aldonic acids besides gluconic, experiments with xylonic acid were also carried out. For the membrane cell experiments, an electrolyte solution with a $MgSO_4$ concentration of 1.5 wt % in DI water was used in the anodic chamber. For this purpose, $MgSO_4$ (1.5 g) was dissolved in DI water, filled up to 100 g, and adjusted to a pH of 2.5 with H_2SO_4. This electrolyte solution was also used to prepare the gold-coated silver wires.

Electrodes. Two different gold-coated silver wires, one of them electrochemically activated (**ECA**), with a geometric surface area of 3.5 cm^2, were used as working electrodes (WEs). The electrochemically activated gold-coated silver wire (**ECA-Au**) was a modified version of the one previously described by Lee *et al.*[37] The **ECA-Au** was prepared by first polishing the silver wire and then cleaning it using cyclic voltammetry (CV, four cycles) in a potential range between −0.2 and −1.2 V *versus* Ag/AgCl (saturated KCl) in the electrolyte solution. The silver wire was rinsed with Milli-Q water and anodized in a 3 M sodium chloride solution at 1 V *versus* Ag/AgCl (saturated KCl) for 90 s. The produced silver chloride on the surface of the silver wire was then electrochemically reduced to porous silver in a 0.5 M sodium hydrogen carbonate solution at −2 V *versus* Ag/AgCl (saturated KCl) for 5 min. The wire was rinsed with Milli-Q water and immersed in a 5 mM $HAuCl_4$ solution (with 0.5 M hydrochloric acid as solvent) for 180 s. The wire was then washed with Milli-Q water, and the CV in the electrolyte solution was repeated.[37]

For the gold-coated silver wire without electrochemical activation, a modified gold coating procedure was used. The silver wire was first polished, and 4 cycles of the CV between −0.2 and −1.2 V *versus* Ag/AgCl (saturated KCl) in the electrolyte solution were performed. The wire was rinsed with Milli-Q water and then immersed in the 5 mM $HAuCl_4$ solution for 90 s. The wire was again washed with Milli-Q water, and the CV in the electrolyte solution was repeated.[37] For comparison of the fabricated gold-coated silver WEs, a pure gold wire was used as a WE. The latter was rinsed with Milli-Q water prior to the reaction.

The platinum mesh used as the counter electrode (CE) was cleaned with nitric acid and rinsed with DI water prior to the reactions. In order to check whether the platinum of the CE inhibits the gold-coated silver electrode, experiments with carbon paper as the CE were carried out. The carbon paper was used without any pretreatment.

Electrochemically Active Surface Area. The electrochemically active surface area (ECSA) of each electrode was determined *via* the electrochemical double-layer capacitance of the electrocatalytic surface. The ECSA was determined *via* a modified version described by Regmi *et al.*[38] The double-layer capacitance was measured *via* CV at different scan rates in the non-Faradaic current range. For the measurements, a 3-electrode setup in a membrane cell was used with a 2.5 wt % gluconic acid solution (G1) with 1.5 wt % $MgSO_4$ as electrolyte and a pH of 2.5 in the chamber with the WE and an electrolyte solution in the CE chamber. The different gold-coated silver electrodes were used as WE. An Ag/AgCl (saturated KCl) electrode acted as the reference electrode and a platinum mesh as CE, respectively. The open-circuit potential (OCP) of the system was determined, and a CV at the potential window OCP ± 0.05 V was performed. The scan rates for the cyclic voltammograms were between 10 and 100 $mV{\cdot}s^{-1}$. The initial potentials of the CV curves were held for 10 s.

Electrocatalysis. The electrochemical reactions were performed using a 3-electrode setup in an undivided and a membrane cell (H-cell). Gold-coated silver wires with different surface areas were used as WE. A platinum mesh and carbon paper acted as the CE and an Ag/AgCl (saturated KCl) as the reference electrode. The reactions were performed at −1.04 V *versus* RHE at different reaction times up to 20 h. The volume loss during the hydrogen evolution reaction (HER) was taken into account when calculating the produced amount of sugars by the subtraction of the measured initial sugar concentration corrected by the volume loss. The configurations of the experiments performed are given in Table 2. An experiment with a gold wire as WE served as reference for comparison. A second reference experiment was performed with the gold-coated silver wire that was not electrochemically activated at a lower pH value (pH = 1) to determine the influence of the H_2SO_4. These reference experiments can be found in the Supporting Information (I. Reference Experiments). In brief, increasing the H_2SO_4 concentration did not lead to higher conversion rates.

Table 2. Summary of Experiments (E1−E8) with the Different AAS with 2.5 wt % Gluconic Acid Concentration (G1) and 2.5 wt % Xylonic Acid Concentration (X1), the Different Cell-Types, the Geometric Area of the WEs [*A*(WE)] Marked with ECA-Au for the Electrochemically Activated One, the Types of CE (Pt: Platinum Mesh, CP: Carbon Paper) and the Reaction Times (RT)

nr.	AAS	cell-type	*A*(WE)/cm^2	CE	RT/h
E1	G1	H	3.5	Pt	20
E2	G1	H	3.5 (ECA-Au)	Pt	1, 2, 4, 6, 8, 20
E3	G1	undivided	3.5	Pt	20
E4	G1	undivided	3.5 (ECA-Au)	Pt	20
E5	X1	H	3.5	Pt	20
E6	X1	undivided	3.5	Pt	20
E7	G1	H	3.5	CP	20
E8	G1	undivided	3.5	CP	20

Mechanism Calculations. ReaxFF molecular dynamics (MD) simulations of the adsorption of xylonic acid onto the gold-coated silver wire electrode in an acidic solution (large model) and quantum chemistry calculations on reduced models extracted from the classical description were used to provide a possible atomistic picture of the xylonic acid-to-xylose conversion mechanism at the electrode surface. A word of caution is needed here. The use of oversimplified models, such as the ones chosen here for the quantum chemistry calculations, to estimate energy barriers for possible mechanisms should be viewed as an attempt to provide a reasonable value in line with the experimental results. Indeed, all the system components, namely the Au layer, the adsorbates, H_2SO_4, water, and their intermolecular interactions, are crucial for identifying the main species involved in the reactions and their dynamics at the electrode interface.

Model Building and ReaxFF MD. The supramolecular arrangement built for this purpose consisted of an Au(111) slab (10 layers of 90 atoms each, 2.5 × 2.5 × 2.5 nm^3),[39,40] 10 xylonic acid molecules, 10 H_2SO_4 molecules, and approximately 700 water molecules. We selected the Au(111) facet because it has been repeatedly studied in our previous reports and is frequently used to represent electrified gold electrodes. All the species were placed inside a simulation box where the size was about 2.5 × 2.5 × 6.0 nm^3 (periodic boundary conditions were applied in all directions). MD simulations based on the reactive force field parametrized in the studies of Monti *et al.*[41,42] were carried out to equilibrate the system at the experimental temperature (298 K—*NVT* ensemble—about 50 ps) and obtain an appropriate packing of all the components (1 atm—*NPT* ensemble—about 50 ps). Then, starting from the final equilibrated structure, the MD simulations (*NVT* ensemble) were extended to sample various configurations of the system and disclose adsorption modes and significant intermolecular interactions leading to the reaction (500 ps). System structures were collected every 0.02 ps, the temperature was controlled through the Berendsen thermostat with a relaxation constant of 0.1 ps, and the time step was set to 0.2 fs. The starting arrangements of xylonic acid were extended chains pointing toward the surface with the carboxylic groups at a close distance (about 4 Å). The xylonic acid chains became adsorbed on the Au interface during equilibration, and only a few maintained the elongated orientation. Indeed, most of them were bent toward the surface, with the OH moieties directly interacting with the gold atoms (Figure S1). Also, H_2SO_4 molecules were strongly connected to the interface through the oxygen atoms, inducing the formation of adatoms and, in a few cases, releasing their hydrogens to the Au atoms nearby. Water molecules were adsorbed too, and the surface was only partially

https://doi.org/10.1021/acssuschemeng.2c05576
ACS Sustainable Chem. Eng. XXXX, XXX, XXX−XXX

covered with the xylonic acid chains (Figures 1 and S2). The production trajectory was analyzed by focusing on atom−atom radial

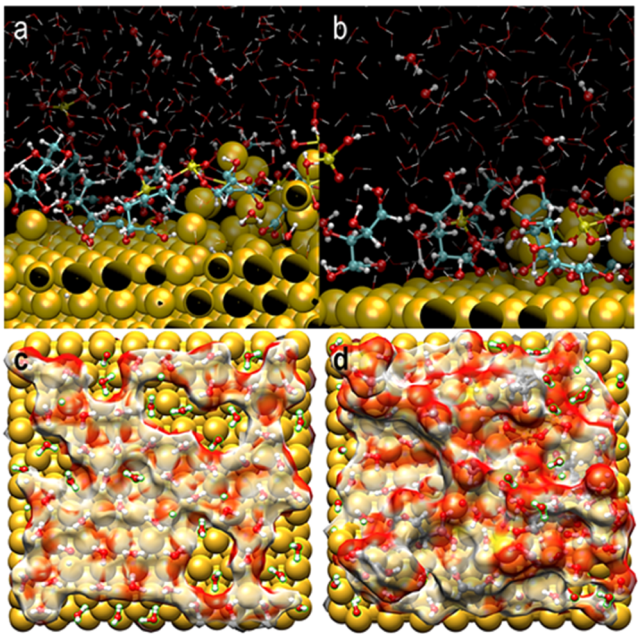

Figure 1. Final configuration (large model) of the MD trajectory at 298 K. Two different views (a,b) of the gold interface (dark yellow spheres) with the adsorbed xylonic acid chains, H_2SO_4, and water molecules. To give an idea of the surface coverage (molecules within 3.5 Å of the surface), both interfaces of the slab are shown in (c) (no xylonic acid adsorbates, only water molecules) and (d) (with adsorbed xylonic acid, water, and H_2SO_4). The adsorbed layers are rendered through a partially transparent solvent-accessible surface. Carbon, oxygen, sulfur, and hydrogen are dark cyan, red, yellow, and white, respectively.

distribution functions (RDFs), spatial distribution functions, and the various adsorption modes of the xylonic acid molecules. The ReaxFF code implemented in the Amsterdam density functional package[43] was employed for all the simulations.

Nudged Elastic Band Simulations. Minimum-energy paths for the acid-to-sugar reaction and activation energies (transition states—TS) were estimated through the nudged elastic band (NEB) methodology[44] implemented in the Quantum Espresso[45] software package. The calculations were based on a plane-wave basis set considering the projector augmented wave method with Perdew−Burke−Ernzerhof functional and kinetic energy cutoffs of 40 and 400 Ry for the wave functions and the charge density, respectively. Single-particle wave functions were calculated through the Gaussian smearing of 0.002 Ry. The Brillouin zone sampling was restricted to the Gamma point, and all the calculations were spin-polarized. Long-range nonlocal effects were included by applying van der Waals corrections (Grimme-D2 approach). The energy barriers were estimated considering eight intermediate images between the selected configurations, and a convergence cut-off of 0.05 eV·Å^{-1} for the force orthogonal to the path was employed.

High-Performance Liquid Chromatography. The concentrations of gluconic acid, xylonic acid, xylose, and glucose were analyzed by ion exchange chromatography. Quantification of the monosaccharides used a Dionex CarboPac SA10 4 × 50 mm as pre-column and a Dionex CarboPac SA10 4 × 250 mm as separation column in combination with a Thermo Scientific ICS 5000+ HPLC system. For gradient elution, DI water and a 0.35 M sodium hydroxide solution were used. The flow rate was 1 mL·min^{-1}, and the injection volume was 10 μL. Pulsed amperometry was used for detection. The aldonic acids were quantified using the same apparatus, but the injection volume was changed to 25 μL, and the eluent was a 0.6 M sodium hydroxide solution.

Scanning Electron Microscopy. The morphology and topography of the wires were analyzed via scanning electron microscopy (SEM) using a JEOL JSM-7000F microscope. SEM micrographs were recorded using an accelerating voltage of 15 kV. An energy-dispersive (EDS) detector was also used to analyze the energy spectrum in order to determine the abundance of specific elements.

X-ray Photoelectron Spectroscopy. X-ray photoelectron spectroscopy (XPS) measurements were performed using a Theta Probe (Thermo Fisher Scientific). A monochromatic Al K_α source at 1386.6 eV was used as the X-ray source. The spectrometer was calibrated to the 368.21 eV binding energy (BE) of the Ag $3d_{5/2}$ line for metallic silver, and linearity was corrected to the BE of 83.96 eV for the Au $4f_{71/2}$ line. An EX05 ion gun with argon cations at 3 keV, 1 μA, and 4 mm^2 was used for sputtering. For all measurements, the lateral resolution of the X-ray spot was set to 400 μm. The pass energy of the detailed spectra for the recording was 50 eV BE, and the survey spectra were recorded with a pass energy of 200 eV BE. The base pressure in the analytical chamber was below 5 × 10^{-8} Pa. The binding states of the elements detected were analyzed using the 2012 NIST XPS database for reference.

RESULTS AND DISCUSSION

The details of the ECSA determination, including the corresponding equations, can be found in the Supporting Information (II. Electrochemically Active Surface Area). The CVs (Figures S3 and S4) and the diagram for the determination of the double-layer capacitance (Figure S5) with the corresponding values (Table S2) are also included in the Supporting Information. The determined ECSA for the gold-coated silver wire with a geometric surface area of 3.5 cm^2 without the electrochemical activation was 26 cm^2. Due to the electrochemical activation of the ECA-Au, the ECSA could be largely increased to over 241 cm^2. From the SEM micrographs of the gold-coated silver electrodes (Figure S6a), it could be observed that the gold coating was not continuous. Nevertheless, the surface area was increased by the recurring coating height of the unconnected gold areas on the surface.

The linear sweep voltammetry (LSV) curves for the experiments performed in different cell types, with xylonic acid and gluconic acid at 2.5 wt % and a WE area of 3.5 cm^2, are depicted in Figure 2. For the experiments of the 2.5 wt % gluconic acid concentration and 1.5 wt % $MgSO_4$ as electrolyte sharper increases in the cathodic current density can be observed in the undivided cell (E3) compared to the H-cell (E1). The same curve shapes can be seen for the experiments with 2.5 wt % xylonic acid with 1.5 wt % $MgSO_4$ as electrolyte and a geometric WE area of 3.5 cm^2 in the undivided cell (E6) and the divided cell (E5). The membrane resistance in the system and the greater distance between the electrodes in the H-cell could have been responsible to this behavior. The LSV experiments were performed without any stirring and, therefore, the current densities at equivalent potentials during the chronoamperometry (CA) were more cathodic. Since a greater cathodic current promotes HER, various potentials were tested, while −1.04 V *versus* RHE was identified as the one with the best conversion of the acid accompanied by tolerable HER.

The sharper increase in the cathodic current density in the divided cell for the xylonic acid was at a cathodic potential over −1.3 V *versus* reversible hydrogen electrode (RHE), which was higher than the one obtained for gluconic acid. The behavior of the xylonic acid in both cell types was more comparable, unlike what was observed for the gluconic acid. For both acids,

https://doi.org/10.1021/acssuschemeng.2c05576
ACS Sustainable Chem. Eng. XXXX, XXX, XXX−XXX

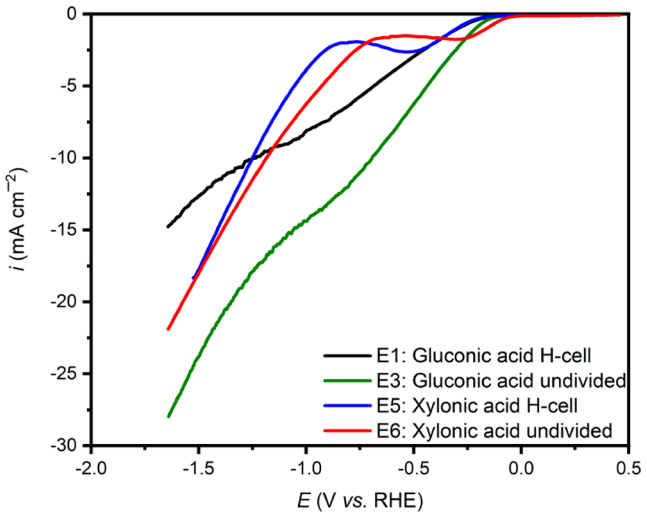

Figure 2. LSV curves of 2.5 wt % gluconic acid solution in an H-cell (E1) and in an undivided cell (E3) and of the 2.5 wt % xylonic acid solution in an H-cell (E5) and an undivided cell (E6). The electrolyte concentration for the solutions was 1.5 wt % $MgSO_4$. The geometric surface area of the not electrochemically activated gold-coated silver WEs was 3.5 cm^2. A scan rate of 10 $mV \cdot s^{-1}$ was used.

the cathodic current density increased faster in the undivided cell, but only for xylonic acid it reached the curve of the H-cell. The reduction reactions in the xylonic acid system needed higher cathodic potentials for the same current densities, which could be due to the equilibrium between the sugar and the corresponding lactone.[46]

The CA curves in Figure 3 illustrate the experiments with 2.5 wt % gluconic acid in the H-cell (E1) and in the undivided cell (E3) and the 2.5 wt % xylonic acid in the H-cell (E5) and in the undivided cell (E6). All of them, with a concentration of 1.5 wt % $MgSO_4$ as electrolyte and WE areas of 3.5 cm^2, behaved similarly in the same cell type. Over time, the current

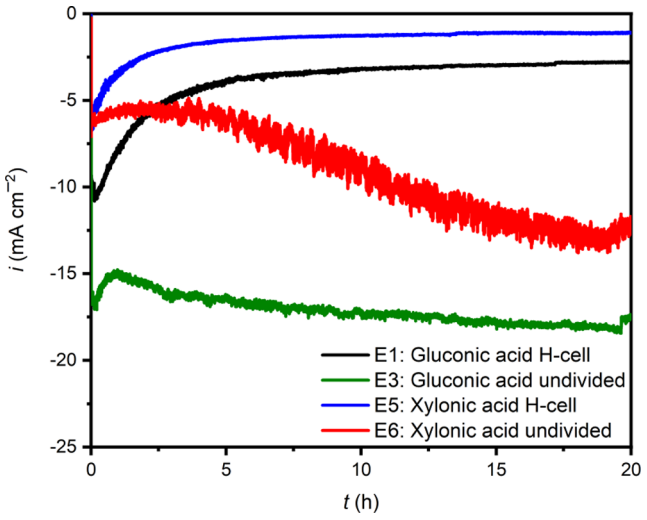

Figure 3. CA curves of the 2.5 wt % gluconic acid solution in an H-cell (E1) and in an undivided cell (E3) and of the 2.5 wt % xylonic acid solution in an H-cell (E5) and an undivided cell (E6). The reactions were performed at −1.04 V *vs* RHE. The electrolyte concentration was 1.5 wt % $MgSO_4$, and the geometric surface area of the not electrochemically activated gold-coated silver WEs was 3.5 cm^2.

density became less cathodic in the experiments with the H-cell, while it became more cathodic in the undivided cell. For the undivided cell with both reactions occurring in the same chamber, the concentration of oxidized species in the reaction media is increased, which makes the bulk concentration variable. The falling current density curve in the undivided cell can be associated to the interactions between the different substances and also to the reduction of the volume because of the oxygen evolution reaction and HER. The higher quantity of gas bubbles in the solutions and their tendency to escape at the surface led to a higher oscillation of the curves for the undivided cell. In addition, the back reaction of gluconic acid to glucose could take place, and the oxidative decarboxylation of the gluconic acid to arabinose could be detected in the undivided cell, which in turn influences the current density.

In the course of all reactions, the conversion of aldonic acids to the corresponding biomass sugars was observed. The initial aldonic acid concentrations, the cell types, the area of the WEs, the aldoses produced, and the conversion rates are listed in Table 3. The calculation of the produced glucose is given in eq 1

$$c(\mathrm{G,\ prod.}) = c(\mathrm{G}) - c_0(\mathrm{G}) \cdot \frac{c(\mathrm{G}) + c(\mathrm{GA})}{c_0(\mathrm{G}) + c_0(\mathrm{GA})} \quad (1)$$

where c(G, prod.) is the produced concentration of glucose ($mmol \cdot L^{-1}$), c(G) is the measured concentration of glucose after the reaction ($mmol \cdot L^{-1}$), c_0(G) is the measured initial concentration of glucose ($mmol \cdot L^{-1}$), c(GA) is the measured gluconic acid concentration ($mmol \cdot L^{-1}$), and c_0(GA) is the initial measured gluconic acid concentration ($mmol \cdot L^{-1}$). The values for the calculations are tabulated in the Supporting Information (Table S3). Xylose production in the H-cell was calculated analogously.

A larger surface area of the WE increased the sugar production (Table 3), which is in agreement with the general knowledge in electrolysis. Compared to the gold-coated silver wire with an ECSA of 26 cm^2, the glucose production reached approximately 2.3 times with the ECA-Au wire with an ECSA of 241 cm^2.

Increased conversion of the substrate and enhanced electrocatalytic performance with a highly porous rather than a planar electrode surface were also observed by Lee *et al.*[37]

In the undivided cell, a higher conversion to glucose could be achieved compared to the divided cell due to the higher current density. In the undivided cell, the oxidative decarboxylation of gluconic acid to arabinose took place as a side reaction. The glucose concentration produced in the gluconic acid experiment in the undivided cell is given by eq 2

$$c(\mathrm{G,\ prod.}) = c(\mathrm{G}) - c_0(\mathrm{G}) \cdot \frac{c(\mathrm{G}) + c(\mathrm{GA}) + c(\mathrm{A})}{c_0(\mathrm{G}) + c_0(\mathrm{GA}) + c_0(\mathrm{A})} \quad (2)$$

where c(G, prod.) is the produced concentration of glucose ($mmol \cdot L^{-1}$), c(G) is the measured concentration of glucose after the reaction ($mmol \cdot L^{-1}$), c_0(G) is the measured initial concentration of glucose ($mmol \cdot L^{-1}$), c(GA) is the measured gluconic acid concentration ($mmol \cdot L^{-1}$), c_0(GA) is the initial measured gluconic acid concentration ($mmol \cdot L^{-1}$), c(A) is the concentration of arabinose ($mmol \cdot L^{-1}$), and c_0(A) is the initial measured arabinose concentration ($mmol \cdot L^{-1}$).

For the xylonic acid experiments, calculations were analogous, replacing gluconic acid with xylonic acid, glucose

https://doi.org/10.1021/acssuschemeng.2c05576
ACS Sustainable Chem. Eng. XXXX, XXX, XXX−XXX

Table 3. Summary of All Experiments (E1−8) with Associated Experiment Abbreviations (E1−E8), Different AA and AA Concentrations *w*(AA), Different Cell Types, Geometric Area of the WEs [*A*(WE)] Marked with ECA-Au for the Electrochemically Activated One, ECSAs, Types of CE (Pt: Platinum Mesh, CP: Carbon Paper), Produced Sugar Concentrations, and Conversion Rates of AA [CR(AA)][a]

nr.	aldonic acid	*w*(AA)/wt %	cell-type	*A*(WE)/cm^2	ECSA/cm^2	CE	*c*(sugar, prod.)/mmol·L^{-1}	CR(AA)/%
E1	gluconic acid	2.5	H	3.5	26	Pt	0.29	0.21
E2	gluconic acid	2.5	H	3.5 (ECA-Au)	241	Pt	0.65	0.43
E3	gluconic acid	2.5	undivided	3.5	26	Pt	1.26	1.32
E4	gluconic acid	2.5	undivided	3.5 (ECA-Au)	241	Pt	0.78	0.66
E5	xylonic acid	2.5	H	3.5	26	Pt	0.06	0.04
E6	xylonic acid	2.5	undivided	3.5	26	Pt	0.35	0.24
E7	gluconic acid	2.5	H	3.5	26	CP	0.08	0.05
E8	gluconic acid	2.5	undivided	3.5	26	CP	0.73	0.84

[a]The reactions were performed at −1.04 V *vs* RHE. All WEs are gold-coated silver wires; ECA stands for electrochemically-activated.

with xylose, and arabinose with threose. The highest conversion rate in the H-cell could be achieved with the ECA-Au. Compared to the gold-coated silver wire with an ECSA of 26 cm^2, the conversion rate increased more than twice. All conversion rates, except for the experiment (E3) in the undivided cell with 2.5 wt % gluconic acid, an electrolyte concentration of 1.5 wt %, and an ECSA of 26 cm^2, were below 1%. However, for this experiment E3 also arabinose was produced as a side-product. In the undivided cell, the conversion rate in the experiment with the ECA-Au as WE with a solution of 2.5 wt % gluconic acid and 1.5 wt % $MgSO_4$ (E4) was onlyapproximately 50% of the gold-coated silver wire that was not previously electrochemically activated. This could be due to the higher conversion of the gluconic acid into the arabinose and also a faster back-reaction of the glucose to the gluconic acid. The conversion rate could not be increased due to the setup limitations of the divided and undivided cells. The timeline experiment (E2) with 2.5 wt % gluconic acid, an electrolyte ($MgSO_4$) concentration of 1.5 wt %, in the H-cell with the ECA-Au showed that the glucose concentration increased over a reaction time of 20 h (Figure 4).

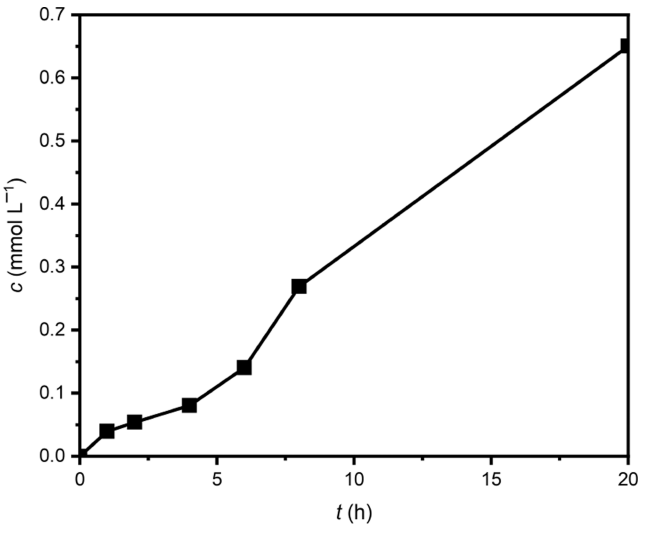

Figure 4. Glucose concentrations produced in the experiment (E2) at a potential of −1.04 V *vs* RHE in an H-cell out of a 2.5 wt % gluconic acid solution with 1.5 wt % $MgSO_4$ and the electrochemically activated gold-coated silver WE (ECA-Au) with a geometric surface area of 3.5 cm^2 over a reaction time of 20 h.

SEM micrographs of the ECA-Au before and after use for a reaction with 2.5 wt % gluconic acid and an electrolyte concentration of 1.5 wt % in the H-cell showed no difference (Figure 5). The micrographs of the 3.5 cm^2 gold-coated silver wire without the electrochemical activation showed also no difference (Figure S6). Hence, the reaction had no measurable effect on the topography and morphology of the WE. While the gold deposits were clearly visible, the SEM and EDS micrographs showed that the coating of the silver wire with gold was not continuous. EDS measurements for both wires (ECA-Au and gold-coated silver wire) showed no significant difference (Table 4). The gold coating on the ECA-Au was less than on the gold-coated silver wire, which could be due to some diffusion limits because of the porous structure of the ECA-Au.

The surface composition of the gold-coated silver wire was also analyzed *via* XPS (with and without sputtering) before and after the reaction (Figure 6). Due to spin−orbit coupling of two main components, $4f_{7/2}$ (84.0 eV) and $4f_{5/2}$ (87.8 eV) are visible in the XPS of Au 4f. The Ag 3d curve also shows two spin−orbit coupling components: $3d_{5/2}$ at 368.2 eV and $3d_{3/2}$ at 474.2 eV. Neither elemental XPS pattern showed significant shifts between the curves before and after the reaction, and thus no effect of the substrate on the electrode surface during the reaction was detected. Because no influence of the reaction on the WE surface could be detected, the WE could be reused for another reaction. Additionally, the electrodes could be recycled by removing the gold layer, that is polishing, and repeating the electroplating of the silver wire with gold.

The possible inhibition of the gold-coated silver electrode by the Pt CE could lead to lower conversion rates to sugars. The inhibition could be due to the oxidation of the Pt to soluble Pt-ions, which could then react with the gold-coated silver electrode. In order to check the influence of Pt on the reaction, experiments with carbon paper as CE were carried out. For each of the two different cell types, an experiment analogous to the one with the highest conversation rate was performed using carbon paper as a CE. The reactions with the carbon paper confirmed that the gold-coated silver electrode was not measurably inhibited by the platinum. In the divided cell, only a quarter of the glucose could be produced using carbon paper as the CE instead of the platinum mesh. In the undivided cell, only 0.58 times of the glucose production could be achieved using carbon paper as an alternative to the platinum mesh as the CE. However, it should be noted that the low

https://doi.org/10.1021/acssuschemeng.2c05576
ACS Sustainable Chem. Eng. XXXX, XXX, XXX−XXX

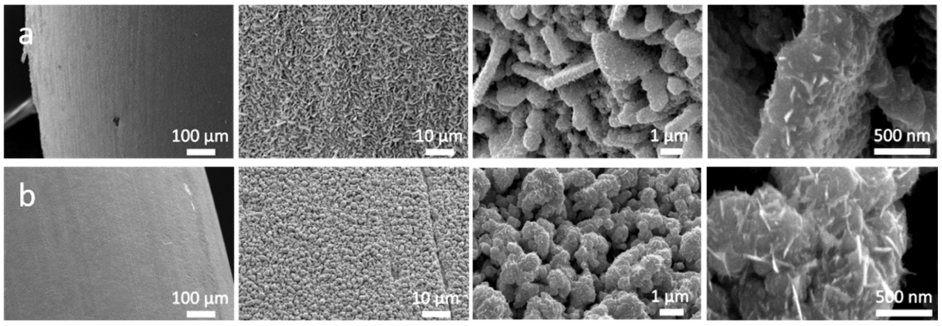

Figure 5. SEM micrographs of the electrochemically activated gold-coated silver wire with a geometric surface area of 3.5 cm^2 (ECA-Au)—(a) before and (b) after reaction with 2.5 wt % gluconic acid and an electrolyte concentration of 1.5 wt % at a potential of −1.04 V *vs* RHE in the H-cell.

Table 4. EDS Measurements of the Electrochemically Activated Gold-Coated Silver Wire with a Geometric Surface Area of 3.5 cm^2 (ECA-Au) and Not Electrochemically Activated Gold-Coated Silver Wire with a Geometric Surface Area of 3.5 cm^2 (GCSE) before and after the Reaction with 2.5 wt % Gluconic Acid and an Electrolyte Concentration of 1.5 wt % in the H-Cell[a]

name		*w*(Au)/wt %	*w*(Ag)/wt %	*x*(Au)/at. %	*x*(Ag)/at. %
ECA-Au	before reaction	40	60	26	74
	after reaction	40	60	27	73
GCSE	before reaction	79	21	87	13
	after reaction	75	25	85	15

[a]The reactions were performed at −1.04 V *vs* RHE. *w*(Au) is the mass concentration of gold, and *w*(Ag) the mass concentration of silver. *x*(Au) is the atomic concentration of gold and *x*(Ag) is the atomic concentration of silver.

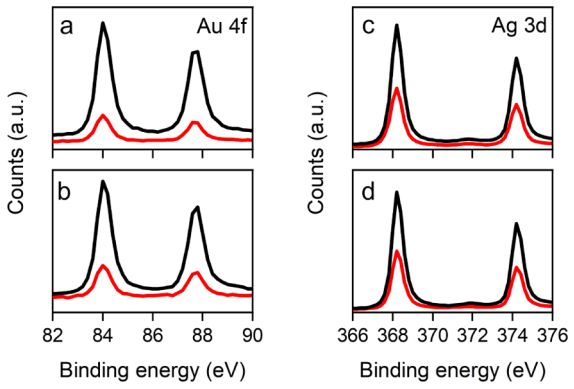

Figure 6. XPS patterns of Au 4f and Ag 3d of the not electrochemically activated gold-coated silver WE with a geometric surface area of 3.5 cm^2. (a) XPS patterns of Au 4f before and (b) after the reaction. (c) XPS patterns of Ag 3d before and (d) after the reaction. The reaction was performed in a 2.5 wt % gluconic acid solution with an electrolyte concentration of 1.5 wt % in the H-cell. The applied potential was −1.04 V *vs* RHE. The black and red lines indicate patterns with and without sputtering, respectively.

mechanical stability of the carbon paper may have decreased the surface area of the CE.

For the results of the mechanism calculations, the examination of the crowded model MD trajectory revealed that many different interactions contributed to stabilizing the xylonic acid molecules on the gold interface due to the affinity of the oxygens to gold and the tendency of the chains to maximize their connections by reorienting the hydroxyls toward the interface (flat adsorption modes). Only a few molecules adopted an almost perpendicular orientation to the substrate, connecting the carboxyl moiety and extending the rest of the chain in the solvent. These chains were also interconnected by hydrogen bonds, surrounded by water and H_2SO_4 that could exchange their hydrogens with the hydroxyl moieties. Furthermore, in agreement with earlier studies, it was found that the adsorption of H_2SO_4 significantly perturbed the structure of the gold surfaces, inducing reconstruction (adatoms). Inspection of the X−Au RDFs shown (Figure S7a) confirms the strong propensity of oxygen to be directly bound to the surface (red, brown, and magenta peaks at about 1.9 Å) and the coordination of the hydroxyl oxygens of xylonic acid to Au (dark cyan peak at about 1.75 Å). Similarly, the tendency of H_2SO_4 to approach the carboxyl oxygens of xylonic acid is proved by the magenta peak at 2.5 Å present in the O(COOH)−O(H_2SO_4) RDF plot of Figure S7b.

Transformations of the xylonic acid into xylose were not observed during these simulations. However, possible intermediate species of these reactions were identified, focusing on the conformations of the adsorbed xylonic acid molecules. The analysis of the data suggests that the relative immobilization of the xylonic acid chains on the electrode surface rendered them prone to interact with the H_2SO_4 nearby molecules, which might transfer their hydrogens to the OH of the carboxyl group strongly adsorbed on the surface through the not-protonated oxygen and, after the release of a water molecule, to the xylonic acid carbon. However, these steps require extra energy that is provided by the electrode. To simulate the reaction in such a complex environment, we resorted to constrained MD simulations and prepared a reduced model by extracting one of the elongated xylonic acid molecules connected to the interface through the carboxyl moiety and the H_2SO_4 close by. The Au(111) slab was reduced to 3 layers of 20 atoms each, 2 H_2SO_4 molecules were selected, and only 64 water molecules were inserted in the simulation box (1.4 × 1.0 × 2.0 nm^3). Constrained MD simulations at T = 298 K in the *NVT* ensemble were performed to transfer the two hydrogens of H_2SO_4 to xylonic acid. The mechanism was fast (0.15 ps)

https://doi.org/10.1021/acssuschemeng.2c05576
ACS Sustainable Chem. Eng. XXXX, XXX, XXX−XXX

(Figure 7), and the energy barriers, estimated from the energy differences (a rough estimate), were around 1.73 eV.

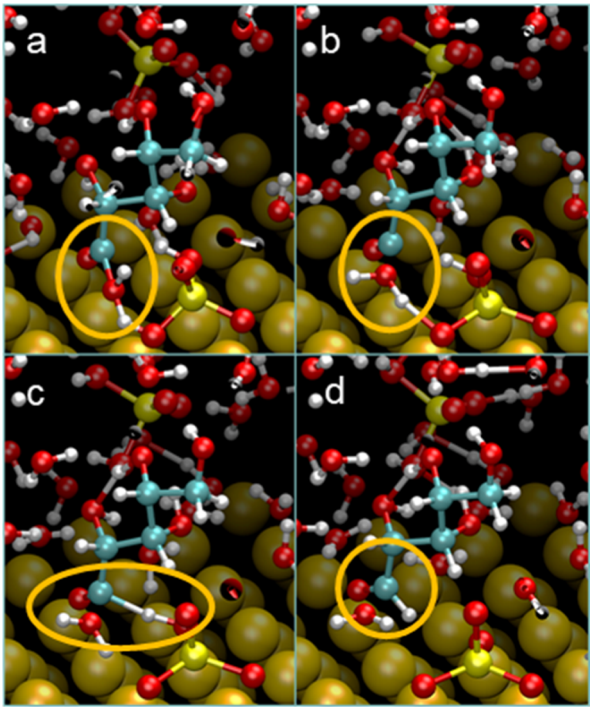

Figure 7. A possible reaction mechanism for converting xylonic acid to xylose could involve a H_2SO_4 molecule adsorbed on the electrode. Au, S, O, C, and H are dark yellow, yellow, red, dark cyan, and white, respectively. (a) Interaction of the proton of the H_2SO_4 with the OH of the carboxyl group, (b) release of the reacted OH of the carboxyl group, (c) interaction of the C of the carboxyl group, which lost the OH before, with the second proton of the H_2SO_4, and (d) finally produced xylose.

We tried the NEB approach at the quantum chemistry level to refine these calculations, further reducing the model system to one molecule of xylonic acid, one molecule of H_2SO_4, and the Au(111) slab frozen at the configuration extracted from the MD trajectory (partially defective surface). Considering many different configurations of reactants and products, broad distributions of energy barriers were found (Figures S8 and S9), with marked peaks between 1.3 and 2.2 eV (in line with the MD estimates) that suggest the simultaneous existence of various reduction mechanisms near the Au surface. In fact, instead of directly transferring the hydrogens from H_2SO_4 to xylonic acid, the mechanism could be carried out by hydrogens released from the gold surface (temporarily adsorbed there) or from H_2 molecules produced by electrolysis. The results of the calculations suggest that the partial immobilization of the acid chains on the electrode favored their conversion to the respective sugar.

CONCLUSIONS

For the reduction of aldonic acids to obtain the corresponding biomass sugars, the use of a gold-coated silver wire as electrocatalyst is presented as a sustainable alternative compared to the traditional hydrothermal reductions. In summary, we have demonstrated a feasible way to electrochemically convert gluconic acid into glucose as an SSL model component. The reduction reaction was not only limited to the sugar with six carbon atoms but also included the reaction of xylonic acid to its corresponding five-carbon sugar xylose. The ECSAs of the electrodes were determined, and the electrochemical reduction was performed both in a membrane cell and in an undivided cell. In the undivided cell, oxidative decarboxylation occurred as a side reaction of the reduction of the aldonic acid. We have shown that a higher conversion rate of the aldonic acids to the corresponding sugars in the H-cell can be achieved with an electrochemically activated gold-coated silver wire (ECA-Au), as well as with an increased reaction time. SEM, EDS, and XPS analyses showed that the surface of the gold-coated silver wire was not affected by the substrates during the reaction. In line with the experimental data, a possible mechanism for the conversion of the xylonic acid to xylose was determined *via* a combination of molecular dynamics simulations and quantum chemistry calculations for a reduced system. The theoretical study indicated that the immobilization of the xylonic acid chains on the electrode surface rendered them prone to interact with the H_2SO_4 nearby molecules. The latter transfer their hydrogens to the OH of the carboxyl group strongly adsorbed on the surface through the not-protonated oxygen and, after the release of a water molecule, to the xylonic acid carbon. Despite the low conversion relative to the used electrode surface, our results show that the aldonic acids can indeed be converted into their corresponding aldoses. This represents a clear breakthrough and an opportunity toward side-stream valorization in industrial processes using green electrons.

ASSOCIATED CONTENT

Supporting Information

The Supporting Information is available free of charge at https://pubs.acs.org/doi/10.1021/acssuschemeng.2c05576.

All measured concentrations, additional information and details of ECSA determination, SEM analysis, computational mechanism characterization details and reference experiments with the experimental data and results (PDF)

AUTHOR INFORMATION

Corresponding Authors

Christian Paulik − *Institute for Chemical Technology of Organic Materials, Johannes Kepler University, 4040 Linz, Austria;* orcid.org/0000-0002-1177-1527; Phone: +43732 24689000; Email: christian.paulik@jku.at

Adam Slabon − *Chair of Inorganic Chemistry, University of Wuppertal, 42119 Wuppertal, Germany;* orcid.org/0000-0002-4452-1831; Phone: +49202 4392517; Email: slabon@uni-wuppertal.de

Authors

Maria Wolfsgruber − *Kompetenzzentrum Holz GmbH, 4860 Lenzing, Austria*

Bruno V. M. Rodrigues − *Chair of Inorganic Chemistry, University of Wuppertal, 42119 Wuppertal, Germany;* orcid.org/0000-0002-0130-8029

Marcia Gabriely da Cruz − *Department of Materials and Environmental Chemistry, Stockholm University, 10691 Stockholm, Sweden*

Robert H. Bischof − *Lenzing AG, 4860 Lenzing, Austria*

Serhiy Budnyk − *AC²T Research GmbH, 2700 Wiener Neustadt, Austria*

https://doi.org/10.1021/acssuschemeng.2c05576
ACS Sustainable Chem. Eng. XXXX, XXX, XXX−XXX

Björn Beele − *Chair of Inorganic Chemistry, University of Wuppertal, 42119 Wuppertal, Germany;* orcid.org/0000-0001-5888-8952

Susanna Monti − *CNR-ICCOM, Institute of Chemistry of Organometallic Compounds, 56124 Pisa, Italy;* orcid.org/0000-0002-3419-7118

Giovanni Barcaro − *CNR-IPCF, Institute of Chemical and Physical Processes, 56124 Pisa, Italy;* orcid.org/0000-0002-5520-5914

Complete contact information is available at: https://pubs.acs.org/10.1021/acssuschemeng.2c05576

Notes

The authors declare no competing financial interest.

■ ACKNOWLEDGMENTS

We would like to acknowledge the Austrian government, the provinces of Lower Austria, Upper Austria, and Carinthia, as well as Lenzing AG, for financial support. Also, we would like to express our gratitude to Johannes Kepler University, Linz, the University of Natural Resources and Life Science (BOKU), Vienna, Stockholm University, the University of Wuppertal and Lenzing AG for their in-kind contributions. Furthermore, we would like to thank the colleague from Wood K+ Markus Huemer, as well as Erwin Malzner, Walter Milacher, and their teams for the support they provided in the laboratories of Lenzing AG. A.S. thanks for additional funding from Vinnova, Sweden's Innovation Agency (project: C1Bio, reference number 2019-03174). S.B. acknowledges the additional financial support by the COMET InTribology project (FFG No. 872176, project coordinator: AC2T research GmbH).

■ REFERENCES

(1) Garedew, M.; Lin, F.; Song, B.; DeWinter, T. M.; Jackson, J. E.; Saffron, C. M.; Lam, C. H.; Anastas, P. T. Greener Routes to Biomass Waste Valorization: Lignin Transformation Through Electrocatalysis for Renewable Chemicals and Fuels Production. *ChemSusChem* **2020**, *13*, 4214−4237.

(2) United Nations Environment Programme. *Land Restoration for Achieving the Sustainable Development Goals: An International Resource Panel Think Piece*; United Nations, 2020.

(3) Schlackl, K.; Bischof, R. H.; Fackler, K.; Samhaber, W. Impact of intermolecular interactions on the nanofiltration of pulping liquor. *Sep. Purif. Technol.* **2020**, *250*, 117177.

(4) Rueda, C.; Calvo, P. A.; Moncalián, G.; Ruiz, G.; Coz, A. Biorefinery options to valorize the spent liquor from sulfite pulping. *J. Chem. Technol. Biotechnol.* **2015**, *90*, 2218−2226.

(5) Fernandes, D. L. A.; Silva, C. M.; Xavier, A. M. R. B.; Evtuguin, D. V. Fractionation of sulphite spent liquor for biochemical processing using ion exchange resins. *J. Biotechnol.* **2012**, *162*, 415−421.

(6) Nigam, J. N. Ethanol production from hardwood spent sulfite liquor using an adapted strain of Pichia stipitis. *J. Ind. Microbiol. Biotechnol.* **2001**, *26*, 145−150.

(7) Cannella, D.; Hsieh, C. C.; Felby, C.; Jørgensen, H. Production and effect of aldonic acids during enzymatic hydrolysis of lignocellulose at high dry matter content. *Biotechnol. Biofuels* **2012**, *5*, 26.

(8) Yu, S.; Wayman, M.; Parekh, S. K. Fermentation to ethanol of pentose-containing spent sulphite liquor. *Biotechnol. Bioeng.* **1987**, *29*, 1144−1150.

(9) Helle, S. S.; Lin, T.; Duff, S. J. Optimization of spent sulfite liquor fermentation. *Enzyme Microb. Technol.* **2008**, *42*, 259−264.

(10) Peters, D. Carbohydrates for fermentation. *Biotechnol. J.* **2006**, *1*, 806−814.

(11) Schlackl, K.; Bischof, R. H.; Samhaber, W. Negative retention by the nanofiltration of aqueous biomass hydrolysates derived from wood pulping. *Sep. Purif. Technol.* **2020**, *242*, 116773.

(12) Fernández-Rodríguez, J.; García, A.; Coz, A.; Labidi, J. Spent sulphite liquor fractionation into lignosulphonates and fermentable sugars by ultrafiltration. *Sep. Purif. Technol.* **2015**, *152*, 172−179.

(13) Pateraki, C.; Ladakis, D.; Stragier, L.; Verstraete, W.; Kookos, I.; Papanikolaou, S.; Koutinas, A. Pretreatment of spent sulphite liquor via ultrafiltration and nanofiltration for bio-based succinic acid production. *J. Biotechnol.* **2016**, *233*, 95−105.

(14) Bhatia, S. K.; Jagtap, S. S.; Bedekar, A. A.; Bhatia, R. K.; Patel, A. K.; Pant, D.; Rajesh Banu, J.; Rao, C. V.; Kim, Y.-G.; Yang, Y.-H. Recent developments in pretreatment technologies on lignocellulosic biomass: Effect of key parameters, technological improvements, and challenges. *Bioresour. Technol.* **2020**, *300*, 122724.

(15) Glattfeld, J. W. E.; Shaver, E. H. The Catalytic Reduction of d-gluconic acid to d-glucose. *J. Am. Chem. Soc.* **1927**, *49*, 2305−2308.

(16) Heikkilä, H.; Puuppo, O.; Tylli, M.; Nikander, H. Verfahren zur Herstellung von Xylitol. EP 0914312 B1, 2002.

(17) Di Marino, D.; Stöckmann, D.; Kriescher, S.; Stiefel, S.; Wessling, M. Electrochemical depolymerisation of lignin in a deep. *Green Chem.* **2016**, *18*, 6021−6028.

(18) Wu, X.; Jiang, J.; Wang, C.; Liu, J.; Pu, Y.; Ragauskas, A.; Li, S.; Yang, B. Lignin-derived electrochemical energy materials and systems. *Biofuels, Bioprod. Biorefin.* **2020**, *14*, 650−672.

(19) Pereira, S. R.; Portugal-Nunes, D. J.; Evtuguin, D. V.; Serafim, L. S.; Xavier, A. M. Advances in ethanol production from hardwood spent sulphite liquors. *Process Biochem.* **2013**, *48*, 272−282.

(20) Anastas, P. T.; Zimmerman, J. B. The periodic table of the elements of green and sustainable chemistry. *Green Chem.* **2019**, *21*, 6545−6566.

(21) Diaz, L. A.; Lister, T. E.; Rae, C.; Wood, N. D. Anion Exchange Membrane Electrolyzers as Alternative for Upgrading of Biomass-Derived Molecules. *ACS Sustainable Chem. Eng.* **2018**, *6*, 8458−8467.

(22) Erythropel, H. C.; Zimmerman, J. B.; de Winter, T. M.; Petitjean, L.; Melnikov, F.; Lam, C. H.; Lounsbury, A. W.; Mellor, K. E.; Janković, N. Z.; Tu, Q.; Pincus, L. N.; Falinski, M. M.; Shi, W.; Coish, P.; Plata, D. L.; Anastas, P. T. The Green ChemisTREE: 20 years after taking root with the 12 principles. *Green Chem.* **2018**, *20*, 1929−1961.

(23) May, A. S.; Biddinger, E. J. Strategies to Control Electrochemical Hydrogenation and Hydrogenolysis of Furfural and Minimize Undesired Side Reactions. *ACS Catal.* **2020**, *10*, 3212−3221.

(24) Park, K.; Pintauro, P. N.; Baizer, M. M.; Nobe, K. Flow Reactor Studies of the Paired Electro-Oxidation and Electroreduction of Glucose. *J. Electrochem. Soc.* **1985**, *132*, 1850−1855.

(25) Pintauro, P. N.; Johnson, D. K.; Park, K.; Baizer, M. M.; Nobe, K. The paired electrochemical synthesis of sorbitol and gluconic acid in undivided flow cells. I. *J. Appl. Electrochem.* **1984**, *14*, 209−220.

(26) Governo, A. T.; Proença, L.; Parpot, P.; Lopes, M.; Fonseca, I. Electro-oxidation of d-xylose on platinum and gold electrodes in alkaline medium. *Electrochim. Acta* **2004**, *49*, 1535−1545.

(27) Bawareth, B.; Di Marino, D.; Nijhuis, T. A.; Jestel, T.; Wessling, M. Electrochemical Membrane Reactor Modeling for Lignin Depolymerization. *ACS Sustainable Chem. Eng.* **2019**, *7*, 2091−2099.

(28) da Cruz, M. G. A.; Gueret, R.; Chen, J.; Piątek, J.; Beele, B.; Sipponen, M. H.; Frauscher, M.; Budnyk, S.; Rodrigues, B. V. M.; Slabon, A. Electrochemical Depolymerization of Lignin in a Biomass-based Solvent. *ChemSusChem* **2022**, *15*, No. e202200718.

(29) Cui, T.; Ma, L.; Wang, S.; Ye, C.; Liang, X.; Zhang, Z.; Meng, G.; Zheng, L.; Hu, H.-S.; Zhang, J.; Duan, H.; Wang, D.; Li, Y. Atomically Dispersed Pt-N3C1 Sites Enabling Efficient and Selective Electrocatalytic C-C Bond Cleavage in Lignin Models under Ambient Conditions. *J. Am. Chem. Soc.* **2021**, *143*, 9429−9439.

(30) Peng, T.; Zhuang, T.; Yan, Y.; Qian, J.; Dick, G. R.; Behaghel de Bueren, J.; Hung, S.-F.; Zhang, Y.; Wang, Z.; Wicks, J.; Garcia de Arquer, F. P.; Abed, J.; Wang, N.; Sedighian Rasouli, A.; Lee, G.; Wang, M.; He, D.; Wang, Z.; Liang, Z.; Song, L.; Wang, X.; Chen, B.;

Ozden, A.; Lum, Y.; Leow, W. R.; Luo, M.; Meira, D. M.; Ip, A. H.; Luterbacher, J. S.; Zhao, W.; Sargent, E. H. Ternary Alloys Enable Efficient Production of Methoxylated Chemicals via Selective Electrocatalytic Hydrogenation of Lignin Monomers. *J. Am. Chem. Soc.* **2021**, *143*, 17226−17235.
(31) Rafiee, M.; Alherech, M.; Karlen, S. D.; Stahl, S. S. Electrochemical Aminoxyl-Mediated Oxidation of Primary Alcohols in Lignin to Carboxylic Acids: Polymer Modification and Depolymerization. *J. Am. Chem. Soc.* **2019**, *141*, 15266−15276.
(32) Schmid, L.; Glaser, F.; Schaer, R.; Wenger, O. S. High Triplet Energy Iridium(III) Isocyanoborato Complex for Photochemical Upconversion, Photoredox and Energy Transfer Catalysis. *J. Am. Chem. Soc.* **2022**, *144*, 963−976.
(33) da Cruz, M. G. A.; Rodrigues, B. V. M.; Ristic, A.; Budnyk, S.; Das, S.; Slabon, A. On the product selectivity in the electrochemical reductive cleavage of 2-phenoxyacetophenone, a lignin model compound. *Green Chem. Lett. Rev.* **2022**, *15*, 153−161.
(34) Caravaca, A.; Garcia-Lorefice, W. E.; Gil, S.; de Lucas-Consuegra, A.; Vernoux, P. Towards a sustainable technology for H2 production: Direct lignin electrolysis in a continuous-flow Polymer Electrolyte Membrane reactor. *Electrochem. Commun.* **2019**, *100*, 43−47.
(35) Rosenbaum, M. A.; Henrich, A. W. Engineering microbial electrocatalysis for chemical and fuel production. *Curr. Opin. Biotechnol.* **2014**, *29*, 93−98.
(36) Huo, Y.; Zeng, H.; Zhang, Y. Integrating Metabolic Engineering and Heterogeneous Chemocatalysis: New Opportunities for Biomass to Chemicals. *ChemSusChem* **2016**, *9*, 1078−1080.
(37) Lee, C.-Y.; Zhao, Y.; Wang, C.; Mitchell, D. R. G.; Wallace, G. G. Rapid formation of self-organised Ag nanosheets with high efficiency and selectivity in CO 2 electroreduction to CO. *Sustainable Energy Fuels* **2017**, *1*, 1023−1027.
(38) Regmi, Y. N.; Roy, A.; King, L. A.; Cullen, D. A.; Meyer, H. M.; Goenaga, G. A.; Zawodzinski, T. A.; Labbé, N.; Chmely, S. C. Lattice Matched Carbide−Phosphide Composites with Superior Electrocatalytic Activity and Stability. *Chem. Mater.* **2017**, *29*, 9369−9377.
(39) Goldsmith, Z. K.; Calegari Andrade, M. F.; Selloni, A. Effects of applied voltage on water at a gold electrode interface from ab initio molecular dynamics. *Chem. Sci.* **2021**, *12*, 5865−5873.
(40) Lin, C.-H.; Ju, S.-P.; Su, J.-W.; Li, D.-E. Peptide Capping Agent Design for Gold (111) Facet by Molecular Simulation and Experimental Approaches. *Sci. Rep.* **2020**, *10*, 2090.
(41) Monti, S.; Carravetta, V.; Ågren, H. Simulation of Gold Functionalization with Cysteine by Reactive Molecular Dynamics. *J. Phys. Chem. Lett.* **2016**, *7*, 272−276.
(42) Monti, S.; Barcaro, G.; Sementa, L.; Carravetta, V.; Ågren, H. Dynamics and self-assembly of bio-functionalized gold nanoparticles in solution: Reactive molecular dynamics simulations. *Nano Res.* **2018**, *11*, 1757−1767.
(43) te Velde, G.; Bickelhaupt, F. M.; Baernds, E. J.; Fonsesca Guerra, C.; van Gisbergen, S. J. A.; Snijders, J. G.; Ziegler, T. *ADF, adf2019.106 SCM: Theoretical Chemistry*; SCM, Virje Universiteit: Amsterdam, The Netherlands, 2001. http://www.scm.com/.
(44) Sheppard, D.; Terrell, R.; Henkelman, G. Optimization methods for finding minimum energy paths. *J. Chem. Phys.* **2008**, *128*, 134106.
(45) Giannozzi, P.; Baroni, S.; Bonini, N.; Calandra, M.; Car, R.; Cavazzoni, C.; Ceresoli, D.; Chiarotti, G. L.; Cococcioni, M.; Dabo, I. QUANTUM ESPRESSO: a modular and open-source software project for quantum simulations of materials. *J. Phys.: Condens. Matter* **2009**, *21*, 395502.
(46) Hummel, M.; Leppikallio, M.; Heikkinen, S.; Niemelä, K.; Sixta, H. Acidity and Lactonization of Xylonic Acid: A Nuclear Magnetic Resonance Study. *J. Carbohydr. Chem.* **2010**, *29*, 416−428.

https://doi.org/10.1021/acssuschemeng.2c05576
ACS Sustainable Chem. Eng. XXXX, XXX, XXX−XXX